Dynamical phase diagram of Gaussian wave packets in optical lattices

H. Hennig,[1,2] T. Neff,[1] and R. Fleischmann[1]
[1]*Max Planck Institute for Dynamics and Self-Organization, 37073 Göttingen, Germany*
[2]*Department of Physics, Harvard University, Cambridge, Massachesetts 02138, USA*
(Received 25 September 2013; revised manuscript received 21 December 2015; published 22 March 2016)

We study the dynamics of self-trapping in Bose-Einstein condensates (BECs) loaded in deep optical lattices with Gaussian initial conditions, when the dynamics is well described by the discrete nonlinear Schrödinger equation (DNLSE). In the literature an approximate dynamical phase diagram based on a variational approach was introduced to distinguish different dynamical regimes: diffusion, self-trapping, and moving breathers. However, we find that the actual DNLSE dynamics shows a completely different diagram than the variational prediction. We calculate numerically a detailed dynamical phase diagram accurately describing the different dynamical regimes. It exhibits a complex structure that can readily be tested in current experiments in BECs in optical lattices and in optical waveguide arrays. Moreover, we derive an explicit theoretical estimate for the transition to self-trapping in excellent agreement with our numerical findings, which may be a valuable guide as well for future studies on a quantum dynamical phase diagram based on the Bose-Hubbard Hamiltonian.

DOI: 10.1103/PhysRevE.93.032219

I. INTRODUCTION

Bose-Einstein condensates (BECs) trapped in periodic optical potentials have proven to be an invaluable tool to study fundamental and applied aspects of quantum optics, quantum computing, and solid state physics [1–5]. In the limit of large atom numbers per well, the dynamics can be well described by a mean-field approximation that leads to a lattice version of the Gross-Pitaevskii equation, the discrete nonlinear Schrödinger equation (DNLSE) [5,6]. One of the most intriguing features of the dynamics of nonlinear lattices is that excitations can spontaneously localize stably even for repulsive nonlinearities. This phenomenon of discrete self-trapping, also referred to as the formation of discrete breathers (DBs), is a milestone discovery in nonlinear science that has sparked many studies (for reviews see [7–9]). Discrete breathers have been observed experimentally in various physical systems such as arrays of nonlinear waveguides [10,11] and Josephson junctions [12,13], spins in antiferromagnetic solids [14,15], and BECs in optical lattices [16]. Self-trapping has also been shown to exist in the dynamics of the Bose-Hubbard Hamiltonian [17] and in calculations beyond the Bose-Hubbard model, which include higher-lying states in the individual wells [18,19].

Under which conditions will a Gaussian distributed initial condition in an optical lattice become diffusive, self-trapped, or a moving breather after sufficient propagation time? This question was addressed in a seminal work [20] that has become a standard reference in both experimental and theoretical studies involving self-trapping in optical lattices including BECs and optical waveguide arrays in the past decade [5,16,21–35]. By means of a variational approach that approximates the DNLSE dynamics, it was shown that the dynamical phase diagram is divided in in different regimes (diffusion, self-trapping, and moving breathers) [20]. The dynamical phase diagram distinguishes between qualitatively different steady-state solutions. However, a recent study [36] indicated that numerical simulations based on the DNLSE show strong deviations from the variational dynamics. Moreover, as we show in Fig. 2(a), the actual parameter regions in which the different dynamical phases can be observed are completely different from those predicted in Ref. [20]. Therefore, an alternative theory of the self-trapping of Gaussian wave packets is needed that can predict the dynamical regimes.

Here we study Gaussian wave packets of BECs in deep optical lattices in the mean-field limit (described by the DNLSE). We present both analytically and numerically a detailed and accurate dynamical phase diagram that separates the different dynamical regimes (diffusion, self-trapping, moving breathers, and multibreathers).

Although our focus is on BECs in optical lattices, where our dynamical phase diagram can be readily probed with single-site addressability [5,23,37], our results apply as well to other systems described by the DNLSE including optical waveguide arrays [21,38]. Our results may as well be a valuable guide for studies that aim to understand the deviations of the correlated self-trapping dynamics as described by the Bose-Hubbard Hamiltonian from the mean-field dynamics. Examples of such deviations have been observed both experimentally [32] and theoretically [17].

II. MODEL

In the limit of large atom numbers per well, the dynamics of dilute Bose-Einstein condensates trapped in deep optical potentials are well described by the mean-field Bose-Hubbard Hamiltonian [6,39,40]

$$H = \sum_{n=1}^{M} U|\psi_n|^4 + \mu_n|\psi_n|^2 - \frac{T}{2}\sum_{n=1}^{M-1}\psi_n^*\psi_{n+1} + \text{c.c.}, \quad (1)$$

where M is the lattice size, $|\psi_n(t)|^2$ is the norm (number of atoms at site n), U denotes the on-site interaction (between two atoms at a single lattice site), μ_n is the on-site chemical potential, and T is the strength of the tunnel coupling between adjacent sites. We use wave functions normalized to the total number of atoms, i.e., $\sum_{n=1}^{M}|\psi_n(t)|^2 = 1$. The corresponding dynamical equation is the DNLSE, which reads

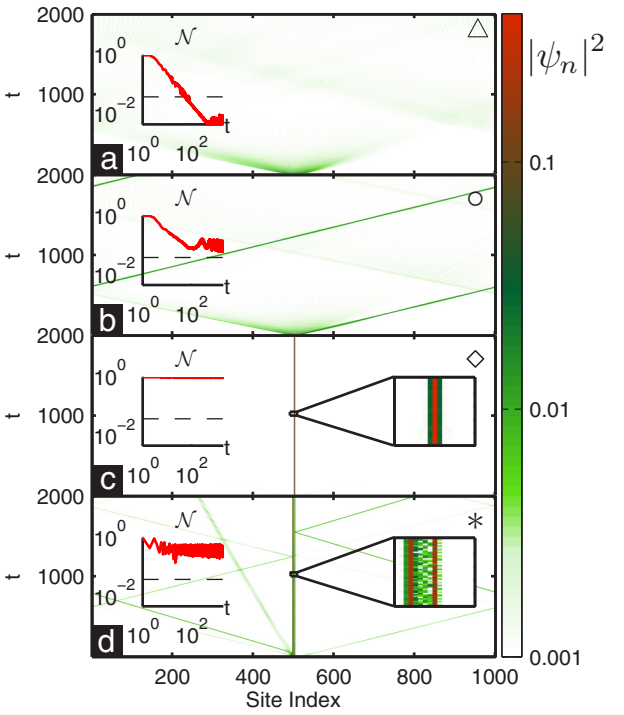

FIG. 1. Examples of the different dynamical regimes and comparison with the variational approach [20]. The density plots show the evolution of the norms $|\psi_n|^2$ of initially Gaussian wave packets (3). The insets on the left show the time traces of the maximum local norm $\mathcal{N}$ [Eq. (6)]. (a) Strongly diffusive regime. In contrast, the variational approach predicts self-trapping. The parameters are $\alpha_0 = 1$, $\cos(p_0) = 0.88$, and $\lambda = 2.5$. (b) Moving breather regime. The variational approach predicts diffusion. The parameters are $\alpha_0 = 1$, $\cos(p_0) = 0.88$, and $\lambda = 1.5$. (c) The DB solution for the parameters $\alpha_0 = 1$, $\cos(p_0) = -1$, and $\lambda = 3$. (d) Breather of higher order with asymmetric shape for the parameters $\alpha_0 = 4$, $\cos(p_0) = -0.6$, and $\lambda = 8.9$. It corresponds to a drop in $\mathcal{H}_{\text{thrs}}$. The examples are indicated by (a) $\triangle$, (b) $\bigcirc$, (c) $\Diamond$ (in Fig. 2), and (d) $*$ (in Fig. 6).

in its dimensionless form

$$i\frac{\partial \psi_n}{\partial t} = (\lambda|\psi_n|^2 + \epsilon_n)\psi_n - \frac{1}{2}[\psi_{n-1} + \psi_{n+1}] \qquad (2)$$

for $n = 1, \ldots, M$, $\lambda = 2U/T$, and $\epsilon_n = \mu_n/T$. In the numerics we present we use periodic boundary conditions ($\psi_{n+1} = \psi_1$), however, we checked that our results hold equally for closed boundary conditions. The DNLSE describes a high-dimensional chaotic dynamical system. Its dynamics, however, is in general far from being ergodic and shows, for example, localization in the form of stationary DBs (localized excitations pinned to the lattice) and so-called moving breathers traversing the lattice [7] (see Fig. 1).

The different characteristic types of dynamics are exemplified in Fig. 1: An initial condition that rapidly disperses, i.e., shows diffusive behavior, can be seen in Fig. 1(a). Moving breathers are strictly speaking not supported by the DNLSE [41]; they radiate from the norm and will eventually be pinned to the lattice or diffusively spread. However, as in Fig. 1(b), these losses of norm can become infinitesimally small so that these solutions remain traveling for extremely long times and can therefore be regarded as actual moving breather solutions for practical use. Finally, an example of a stationary DB emerging from a Gaussian initial condition is shown in Fig. 1(c).

Exact DB solutions were calculated analytically in Refs. [7,42] for a system of three sites (trimer). For larger lattices the DB solutions can be calculated numerically using the anticontinuous method [7,43,44] or a Newton method [45]. Preparation of an experimental system in exact breather states is usually not feasible in practice. In contrast, Gaussian initial conditions, for which we derive a dynamical phase diagram, can be well controlled in experiments on BECs with single-site addressability [5,23,37].

III. VARIATIONAL APPROACH

In Refs. [20,39] the dynamics of Gaussian wave packets defined by

$$\psi_{n,0} \propto \exp\left[-\frac{(n-\xi_0)^2}{\alpha_0} + ip_0(n-\xi_0) + i\frac{\delta_0}{2}(n-\xi_0)^2\right] \qquad (3)$$

was studied using a variational collective coordinate approach (a technique very successfully applied in a variety of fields [46,47]). Here ξ_0 and α_0 are the center and the width of the Gaussian distribution and p_0 and δ_0 their associated momenta. The variational approach leads to approximate equations of motion for the conjugate variables (p,ξ) and $(\delta,\sqrt{\alpha})$ [20,39]. It is important to note that the variational approach assumes that the excitation is well approximated by a Gaussian at *all* times. The effective (approximate) Hamiltonian is [39]

$$H = \frac{\lambda}{2\sqrt{\pi\alpha}} - \cos(p)e^{-\eta}, \qquad (4)$$

with $\eta = \frac{1}{2\alpha} + \frac{\alpha\delta^2}{8}$ depending on the initial values of the center ξ_0 and width parameter $\sqrt{\alpha_0}$ as well as p_0 and δ_0 their conjugate momenta.

In Ref. [20] a dynamical phase diagram was derived based on the variational approach (4). These theoretical predictions, however, disagree with our numerical simulations of the actual DNLSE dynamics, because the final dynamical state will in most cases be highly non-Gaussian. Hence, the variational approach breaks down, e.g., Fig. 1(a) shows diffusion, while the variational approach predicts a self-trapped state. In Fig. 1(b) we find a moving breather while the variational approach yields diffusive behavior. Moreover, the entire phase diagram in Fig. 2(b) (top) for the DNLSE is completely different from the prediction of the variational approach [shown as dashed and dotted lines in Fig. 2(a)].

IV. NUMERICAL CONSTRUCTION OF THE PHASE DIAGRAM

In order to construct a dynamical phase diagram based on the DNLSE, criteria to distinguish the different dynamical regimes are needed. This separation is nontrivial, as part of the atom cloud can, e.g., remain trapped in one region while another part diffuses in the remainder of the lattice. We can separate the regimes by first defining a local norm and local

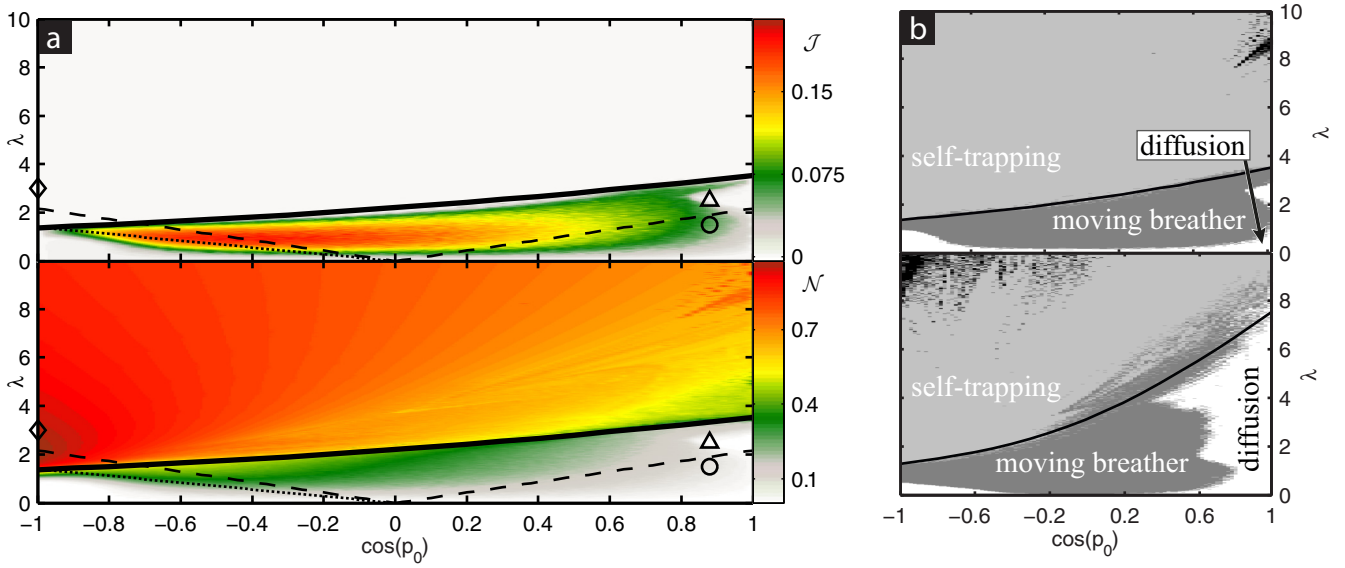

FIG. 2. (a) Construction of the dynamical phase diagram to identify diffusion, self-trapping, and solitons based on two order parameters $\mathcal{J}$ (top) and $\mathcal{N}$ (bottom), compared with our analytical estimate (9) (thick black line) for the transition to self-trapping ($\alpha_0 = 1$). The variational approach [20] (shown here as dashed and dotted lines) fails to predict the different regimes accurately: Above the dashed line all states were predicted to be self-trapped. In the region (for cos $p < 0$) between the dashed and dotted lines moving breathers should occur. The remainder would be the diffusive regime. In fact, we find that the dashed and dotted lines do not at all mark any of the transitions between the different dynamical regimes. Examples of the dynamics for three points in the phase diagram marked with the symbols △, ◯, and ♢ are shown in Fig. 1. (b) Dynamical phase diagram of Gaussian initial conditions in the DNLSE separating diffusion (white), self-trapping (light gray), moving breathers (dark gray), and higher-order self-trapping (multibreathers) (black). The black line represents our analytical estimate (9) of the onset of self-trapping for $\alpha_0 = 1$ (top) and $\alpha_0 = 4$ (bottom) and is in excellent agreement with the numerical data. The other parameters are $M = 1001$ and $\varepsilon = 1.37$.

average current

$$N_{\mathrm{loc}}(x) = \sum_{n=x-a}^{x+a} |\psi_n|^2,$$

$$j_{\mathrm{loc}}(x) = \frac{1}{2}\left| \sum_{n=x-a}^{x+a} \mathrm{Im}[\psi_{n+1}\psi_n^* - \psi_n^*\psi_{n-1}] \right|, \qquad (5)$$

where the parameter a was chosen to be the smallest integer larger than or equal to $\sqrt{\alpha_0}$. From these quantities we construct two order parameters by

$$\mathcal{N} = \left\langle \max_x [N_{\mathrm{loc}}(x)] \right\rangle, \quad \mathcal{J} = \langle j_{\mathrm{loc}}(x_{\max}) \rangle, \qquad (6)$$

where $x_{\max}$ is the central site at which $N_{\mathrm{loc}}(x)$ assumes its maximum. Both quantities were evaluated at time $\tau = 10\,000$ and averaged over the last 10% of the time.

In the diffusive regime both order parameters are small. Moving breathers are characterized by large $\mathcal{N}$ and large $\mathcal{J}$, while in the self-trapping regime one finds large $\mathcal{N}$ but nearly vanishing currents $\mathcal{J}$ due to the stationarity of the self-trapping solutions. Figure 2 shows $\mathcal{J}$ and $\mathcal{N}$ as a function of the initial phase difference p_0 and the nonlinearity λ for $\alpha_0 = 1$ (see the Appendix 3 for $\alpha_0 = 4$). The examples of Fig. 1 are marked in Fig. 2 by different symbols to demonstrate how the above criteria can be used to distinguish the dynamical regimes [a cut along $\cos(p_0) = 0.88$ can be found in the Appendix 1].

We construct the dynamical phase diagram, which assigns every initial condition to a specific dynamical regime by defining suitable thresholds for the order parameters $\mathcal{N}$ and $\mathcal{J}$. Figure 2(a) (top) shows remarkably sharp transitions in the maximum local probability current. We use the thresholds $\mathcal{J}_{\mathrm{thrs}} = 0.002$ to separate moving breathers from self-trapping and diffusion and $\mathcal{N}_{\mathrm{thrs}}$ to delimit diffusion from self-trapping. By setting a threshold $p_T = 10^{-4}$ for the probability density function of $\mathcal{N}$ to be observed in a diffusive state (see the Appendix 2 for details), we find $\mathcal{N}_{\mathrm{thrs}} = 0.028$ for $\alpha_0 = 1$ and $\mathcal{N}_{\mathrm{thrs}} = 0.032$ for $\alpha_0 = 4$.

With these thresholds we obtain the dynamical phase diagram shown in Fig. 2(b). Our results are not sensitive to the exact value of the parameter p_T. For comparison we show a phase diagram obtained with $p_T = 10^{-5}$ in the Appendix 2, which differs only minimally from Fig. 2(b). To identify higher-order self-trapped excitations of more complex structure [see Fig. 1(d)] in our dynamical phase diagram, we use a third-order parameter, the local energy $H_{\mathrm{loc}}(x) = \sum_{n=x-a}^{x+a} \frac{\lambda}{2}|\psi_n|^4 - \sum_{n=x-a-1}^{x+a} \frac{1}{2}(\psi_n^*\psi_{n+1} + \mathrm{c.c.})$ in the vicinity of $x_{\max}$ measured relative to the fixed point energy H_{CP} (which will be introduced below), i.e., $\mathcal{H}(\lambda) = H_{\mathrm{loc}}(x_{\max})/H_{\mathrm{CP}}(\lambda, 1)$. For higher-order self-trapping we found $\mathcal{H} \ll 1$ in contrast to $\mathcal{H} \approx 1$ for discrete breathers centered around a single site. We chose $\mathcal{H}_{\mathrm{thrs}} = 0.8$ and marked this regime in black in Fig. 2(b).

V. THEORY

In the following we derive an analytical estimate for the self-trapping transition separating the different phases in the

dynamical phase diagram. The exact DB solution forming a single peak centered at a single lattice site (denoted by CP for central peak) is a local maximum in the energy and can be numerically constructed using the methods described in Refs. [7,43–45]. The CP solutions correspond to elliptic fixed points in phase space [48], which are separated from moving and chaotic solutions by saddle points in the energy landscape. These saddle points correspond to another kind of stationary solution centered between two lattice sites called central bond (CB) states. They are unstable [48] and have lower energy than CP solutions. Due to continuity, the CB solutions are considered intermediate states for an excitation to hop between lattice sites.

A necessary condition for self-trapping is $H_G \geqslant H_{\mathrm{CB}}$, where H_G is the energy of the initial Gaussian function and H_{CB} is the energy of the CB solution. Since, however, the self-trapped solution is non-Gaussian, only a fraction n of the full norm will be self-trapped. We therefore have to consider the energy H_{CB} of a central-bond state with norm $n < 1$. To this aim we note that the energy of an arbitrary state of norm n compared to the state of the same shape but of unit norm scales as $E(\lambda,n) = nE(\lambda n,1)$. Thus H_{CB} reads

$$H_{\mathrm{CB}}(\lambda,n) = nH_{\mathrm{CB}}(\lambda n,1) = \frac{\Lambda}{\lambda} H_{\mathrm{CB}}(\Lambda,1), \tag{7}$$

with $\Lambda = \lambda n$. We approximate the energy of the initial Gaussian by $H_G = \frac{\lambda}{2\sqrt{\pi\alpha_0}} - \cos(p_0)e^{-\eta_0}$, with $\eta_0 = \frac{1}{2\alpha_0}$ [see Eq. (4)], which we found agrees very well with the energy H of the DNLSE Hamiltonian (1), although the dynamics strongly differs.

We make the following ansatz to estimate the critical nonlinearity λ_c at the transition to self-trapping:

$$H_{\mathrm{CB}}(\lambda_c,n_c) = \frac{\Lambda_c}{\lambda_c} H_{\mathrm{CB}}(\Lambda_c,1) = \frac{\varepsilon}{\lambda_c} \stackrel{!}{=} H_G(\lambda_c), \tag{8}$$

where $\varepsilon = \Lambda_c H_{\mathrm{CB}}(\Lambda_c,1)$ and $\Lambda_c = \lambda_c n_c$. The critical nonlinearity at the transition to self-trapping reads

$$\lambda_c(p_0) = e^{-\eta}\sqrt{\pi\alpha_0}\cos p_0 + \sqrt{e^{-2\eta}\pi\alpha_0\cos^2 p_0 + 2\varepsilon\sqrt{\pi\alpha_0}}. \tag{9}$$

Our analytical estimate of the self-trapping transition (9) is shown in Fig. 2(a) (thick black line) and Fig. 2(b) (thick red line) and is in excellent agreement with the simulations of the DNLSE dynamics. By fixing $p_0 = \pi$ we can determine the constant ε numerically. We find $\lambda_c(p_0) \approx 1.35$ and $\varepsilon_{\mathrm{num}} = 1.375$. We choose $p_0 = \pi$ for the estimate since the phase difference between neighboring sites for an exact solution of a discrete breather is π. Below we will present an independent way to obtain ε by calculating Λ_c directly.

How can we interpret the rescaled nonlinearity Λ_c in Eq. (8)? The ability of localized excitations to move inside a lattice can be analyzed using the concept of the Peierls-Nabarro (PN) energy barrier, which we briefly review: A crucial condition for a localized excitation to move across the lattice is that the initial energy is lower than the energy of a CB solution such that this intermediate state cannot act as a barrier.

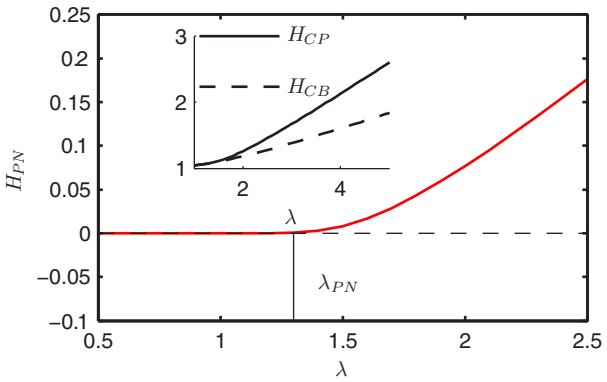

FIG. 3. The onset of a nonzero PN barrier H_{PN} is found at nonlinearity $\lambda_{\mathrm{PN}} \approx 1.3$ (for $n = 1$). The PN barrier H_{PN} is calculated as the difference between the energies of a CP breather (located around a single site) and a CB breather (located between two lattice sites).

Self-trapping, on the other hand, requires the initial energy to be between the maximum energy state CP and CB, which can thus act as a barrier in phase space and inhibits migration. This energy gap H_{PN} between the CP and CB is referred to as the PN barrier [42,48,49].

We report the PN barrier in Fig. 3. Self-trapping requires a nonzero PN barrier, which we find for nonlinearities larger than $\lambda_{\mathrm{PN}} \approx 1.3$ in Fig. 3. Since the transition to self-trapping is reflected by the onset of a nonzero PN barrier, we identify $\Lambda_C \equiv \lambda_{\mathrm{PN}}$. With $H_{\mathrm{CB}}(\lambda_{\mathrm{PN}},1) \approx 1.0723$ we find $\varepsilon = 1.37$ in excellent agreement with the numerical value $\varepsilon_{\mathrm{num}}$. Note that only a fraction of the norm of the initial Gaussian will actually be trapped when a breather is created (and this norm is smaller the more the phase difference p_0 of the Gaussian function deviates from the phase difference of the breather fixed point, i.e., $p = \pi$). Our theoretical analysis focuses on the self-trapped fraction of the norm and thus the existence of a nonzero PN barrier corresponding to the respective fraction of the norm n. This of course leaves the background unattended yet proves to be a valid approximation.

VI. CONCLUSION

We calculated a dynamical phase diagram for the different dynamical regimes (diffusion, moving breathers, and self-trapping) of Gaussian initial conditions in periodic optical potentials. By defining two order parameters, the maximum local atomic density and the maximum local current, we constructed numerically the dynamical phase diagram. We derived an explicit expression (9) for the nonlinear interaction λ_c that separates the dynamical regimes, in very good agreement with the numerical results. Gaussian initial conditions can be well controlled in experiments on BECs with single-site addressability [5,23,37], where our predictions can be readily tested experimentally. We hope our study further stimulates experiments and theoretical work on the transition between self-trapping, diffusion, and solitons in the quantum regime, e.g., based on the Bose-Hubbard Hamiltonian.

ACKNOWLEDGMENTS

We thank Jérôme Dorignac and David K. Campbell for useful discussions.

APPENDIX

1. A cut through the dynamical phase diagram

The dynamical phase diagram of Fig. 2 shows a remarkable transition from diffusive to moving breather behavior back to diffusive motion and then to self-trapping for $\cos(p_0) \approxeq 0.88$. In Fig. 4 we shows curves of the order parameters as a function of the nonlinearity λ for $\cos(p_0) = 0.88$, illustrating the sharp features in the order parameters at the transitions between the different regimes.

2. Definition of the threshold $\mathcal{N}_{\text{thrs}}$

In order to find a suitable upper threshold of the maximal local norm in the diffusive regime we calculate the cumulative probability density function (PDF) of $\mathcal{N}$ in the diffusive case where the single-site norms are known to be exponentially distributed $p = Me^{-Mx}$ [50]. Assuming statistical independents in this regime gives the PDF of the maximum single-site norm as $p_{\max} = M^2[1 - \exp(-Mx)]^{M-1} \exp(-Mx)$. A DB, however, is localized over several sites around the maximum. Therefore, we need to calculate the PDF of the local norm within a range of a sites on either side of the maximum. The PDF of the sum of two single-site norms is given by the convolution of the two PDFs. For r sites with exponentially distributed norms we can thus calculate the PDF of norms iteratively by $p_r = p_{r-1} * p$, where the asterisk denotes convolution. The PDF of the local norm in the range of $2a$ sites around the maximum can consequently be expressed as $p_{\mathcal{N}} = p_{2a} * p_{\max}$. Let us examine an initial condition that leads to vanishing current $\mathcal{J}$. We will consider it to be self-trapped if its evolution leads to a maximum local norm $\mathcal{N}$ that is sufficiently unlikely to be found in the diffusive state. We define as the threshold $\mathcal{N}_{\text{thrs}}$ the norm for which the PDF falls below $p_T = 10^{-4}$. We find $\mathcal{N}_{\text{thrs}} = 0.028$ for $\alpha_0 = 1$ and $\mathcal{N}_{\text{thrs}} = 0.032$ for $\alpha_0 = 4$. However, our results are not sensitive to the exact value of this parameter p_T. Assuming

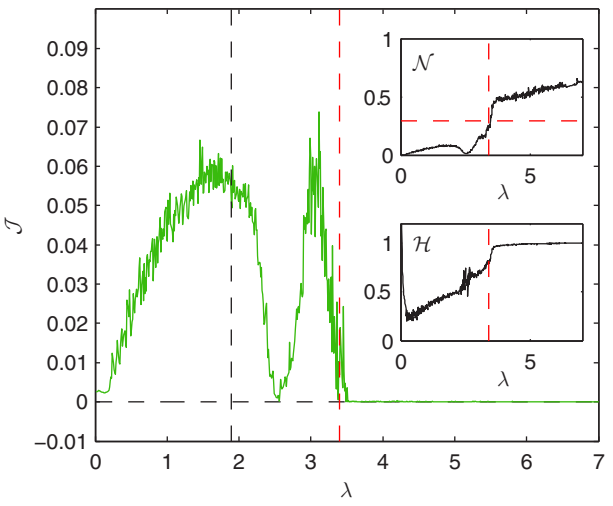

FIG. 4. Cross section through Fig. 2 at $\cos(p_0) = 0.88$. The black vertically dashed line corresponds to the predicted transition between the moving breather and the DB regime of [20] and the red vertically dashed lines indicate our prediction (9). The horizontal red line in the inset for $\mathcal{N}_{\text{thrs}}$ denotes the critical norm at the transition from our analytics, in very good agreement with the numerical data.

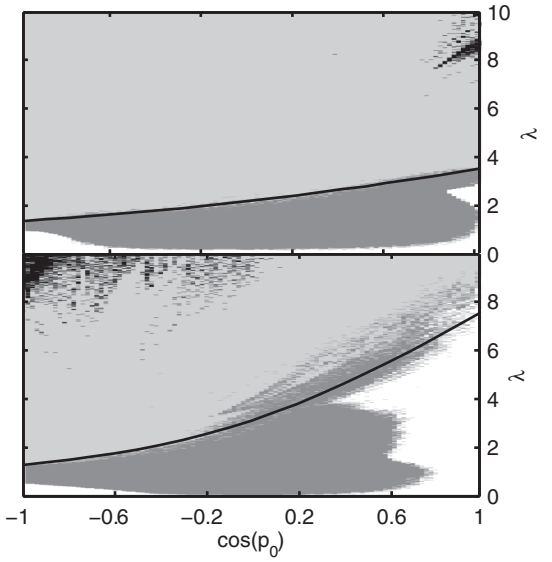

FIG. 5. Dynamical phase diagram for $M = 1001$ and $\alpha_0 = 1$ (top) and $M = 1001$ and $\alpha_0 = 4$ (bottom) obtained with a PDF threshold of the maximum local norm of $p_T = 10^{-5}$.

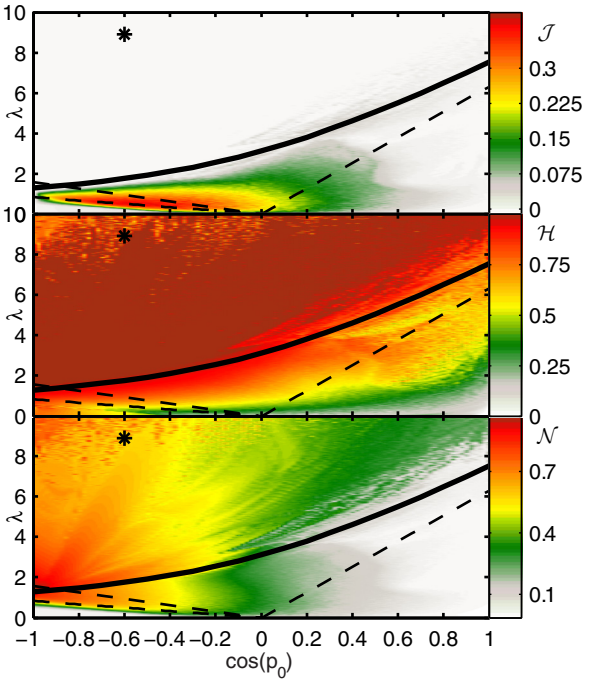

FIG. 6. Color map of the three parameters $\mathcal{J}$ (top), $\mathcal{H}$ (middle), and $\mathcal{N}$ (bottom) for $\sqrt{\alpha_0} = a = 2$ and system size $M = 1001$. The black dashed lines were predicted in Ref. [20] to mark the transition between different dynamical regimes. The solid line is our analytical estimate of the transition between the moving breather and the self-trapping regime [Eq. (9)].

$p_T = 10^{-5}$ yields $\mathcal{N}_{\text{thrs}} = 0.031$ for $\alpha_0 = 1$ and $\mathcal{N}_{\text{thrs}} = 0.035$ for $\alpha_0 = 4$, which result in the dynamical phase diagrams shown in Fig. 5, which differ only minimally from those of Fig. 2(b).

3. Order parameters for $\alpha = 4$

Figure 6 shows the three order parameters $\mathcal{J}$, $\mathcal{H}$, and $\mathcal{N}$ for $\alpha = 4$, which give rise to the dynamical phase diagram for $\alpha = 4$ [see Fig. 2(b) (bottom)].

[1] I. Bloch, Nat. Phys. **1**, 23 (2005).
[2] W. S. Bakr, J. I. Gillen, A. Peng, S. Fölling, and M. Greiner, Nature (London) **462**, 74 (2009).
[3] W. S. Bakr, A. Peng, M. E. Tai, R. Ma, J. Simon, J. I. Gillen, S. Fölling, L. Pollet, and M. Greiner, Science **329**, 547 (2010).
[4] J. Simon, W. S. Bakr, R. Ma, M. E. Tai, P. M. Preiss, and M. Greiner, Nature (London) **472**, 307 (2011).
[5] O. Morsch and M. Oberthaler, Rev. Mod. Phys. **78**, 179 (2006).
[6] C. J. Pethick and H. Smith, *Bose-Einstein Condensation in Dilute Gases* (Cambridge University Press, Cambridge, 2008).
[7] S. Flach and A. V. Gorbach, Phys. Rep. **467**, 1 (2008).
[8] D. K. Campbell, S. Flach, and Y. S. Kivshar, Phys. Today **57**(1), 43 (2004).
[9] H. Hennig and R. Fleischmann, Phys. Rev. A **87**, 033605 (2013).
[10] H. S. Eisenberg, Y. Silberberg, R. Morandotti, A. R. Boyd, and J. S. Aitchison, Phys. Rev. Lett. **81**, 3383 (1998).
[11] R. Morandotti, U. Peschel, J. S. Aitchison, H. S. Eisenberg, and Y. Silberberg, Phys. Rev. Lett. **83**, 2726 (1999).
[12] E. Trías, J. J. Mazo, and T. P. Orlando, Phys. Rev. Lett. **84**, 741 (2000).
[13] A. V. Ustinov, Chaos **13**, 716 (2003).
[14] U. T. Schwarz, L. Q. English, and A. J. Sievers, Phys. Rev. Lett. **83**, 223 (1999).
[15] M. Sato and A. J. Sievers, Nature (London) **432**, 486 (2004).
[16] B. Eiermann, T. Anker, M. Albiez, M. Taglieber, P. Treutlein, K.-P. Marzlin, and M. K. Oberthaler, Phys. Rev. Lett. **92**, 230401 (2004).
[17] H. Hennig, D. Witthaut, and D. K. Campbell, Phys. Rev. A **86**, 051604 (2012).
[18] K. Sakmann, A. I. Streltsov, O. E. Alon, and L. S. Cederbaum, Phys. Rev. Lett. **103**, 220601 (2009).
[19] M. Trujillo-Martinez, A. Posazhennikova, and J. Kroha, Phys. Rev. Lett. **103**, 105302 (2009).
[20] A. Trombettoni and A. Smerzi, Phys. Rev. Lett. **86**, 2353 (2001).
[21] D. N. Christodoulides, F. Lederer, and Y. Silberberg, Nature (London) **424**, 817 (2003).
[22] J. W. Fleischer, M. Segev, N. K. Efremidis, and D. N. Christodoulides, Nature (London) **422**, 147 (2003).
[23] M. Albiez, R. Gati, J. Fölling, S. Hunsmann, M. Cristiani, and M. K. Oberthaler, Phys. Rev. Lett. **95**, 010402 (2005).
[24] F. S. Cataliotti, S. Burger, C. Fort, P. Maddaloni, F. Minardi, A. Trombettoni, A. Smerzi, and M. Inguscio, Science **293**, 843 (2001).
[25] J. W. Fleischer, T. Carmon, M. Segev, N. K. Efremidis, and D. N. Christodoulides, Phys. Rev. Lett. **90**, 023902 (2003).
[26] O. Morsch, J. H. Müller, M. Cristiani, D. Ciampini, and E. Arimondo, Phys. Rev. Lett. **87**, 140402 (2001).
[27] S. Burger, K. Bongs, S. Dettmer, W. Ertmer, K. Sengstock, A. Sanpera, G. V. Shlyapnikov, and M. Lewenstein, Phys. Rev. Lett. **83**, 5198 (1999).
[28] A. Smerzi, A. Trombettoni, P. G. Kevrekidis, and A. R. Bishop, Phys. Rev. Lett. **89**, 170402 (2002).
[29] T. Anker, M. Albiez, R. Gati, S. Hunsmann, B. Eiermann, A. Trombettoni, and M. K. Oberthaler, Phys. Rev. Lett. **94**, 020403 (2005).
[30] R. Iwanow, R. Schiek, G. I. Stegeman, T. Pertsch, F. Lederer, Y. Min, and W. Sohler, Phys. Rev. Lett. **93**, 113902 (2004).
[31] B. Eiermann, P. Treutlein, T. Anker, M. Albiez, M. Taglieber, K.-P. Marzlin, and M. K. Oberthaler, Phys. Rev. Lett. **91**, 060402 (2003).
[32] A. Reinhard, J.-F. Riou, L. A. Zundel, D. S. Weiss, S. Li, A. M. Rey, and R. Hipolito, Phys. Rev. Lett. **110**, 033001 (2013).
[33] C. Bersch, G. Onishchukov, and U. Peschel, Phys. Rev. Lett. **109**, 093903 (2012).
[34] A. Dienst, E. Casandruc, D. Fausti, L. Zhang, M. Eckstein, M. Hoffmann, V. Khanna, N. Dean, M. Gensch, and S. Winnerl, Nat. Mater. **12**, 535 (2013).
[35] G. Dong, J. Zhu, W. Zhang, and B. A. Malomed, Phys. Rev. Lett. **110**, 250401 (2013).
[36] R. Franzosi, R. Livi, G. Oppo, and A. Politi, Nonlinearity **24**, R89 (2011).
[37] T. Gericke, P. Würtz, D. Reitz, T. Langen, and H. Ott, Nat. Phys. **4**, 949 (2008).
[38] D. N. Christodoulides and E. D. Eugenieva, Phys. Rev. Lett. **87**, 233901 (2001).
[39] A. Trombettoni and A. Smerzi, J. Phys. B **34**, 4711 (2001).
[40] P. Buonsante and V. Penna, J. Phys. A **41**, 175301 (2008).
[41] O. F. Oxtoby and I. V. Barashenkov, Phys. Rev. E **76**, 036603 (2007).
[42] H. Hennig, J. Dorignac, and D. K. Campbell, Phys. Rev. A **82**, 053604 (2010).
[43] S. Aubry, Physica D **103**, 201 (1997).
[44] J. Marin and S. Aubry, Nonlinearity **9**, 1501 (1996).
[45] L. Proville and S. Aubry, Eur. Phys. J. B **11**, 41 (1999).
[46] D. Campbell, J. Schonfeld, and C. Wingate, Physica D **9**, 1 (1983).
[47] D. K. Campbell, Ann. Phys. (N.Y.) **129**, 249 (1980).
[48] B. Rumpf, Phys. Rev. E **70**, 016609 (2004).
[49] Y. S. Kivshar and D. K. Campbell, Phys. Rev. E **48**, 3077 (1993).
[50] G. S. Ng, H. Hennig, R. Fleischmann, T. Kottos, and T. Geisel, New J. Phys. **11**, 073045 (2009).